 doi:10.20944/preprints202107.0119.v1

Article

Copper, Iron and Aluminium Electrochemical Corrosion Rates and Intrinsic Diffusivitives Dependence on Temperature Investigations

Mykhaylo V. Yarmolenko

Kyiv National University of Technologies and Design, Faculty of Market, Information and Innovation Technologies, Cherkasy, Ukraine, e-mail: yarmolenko.mv@knutd.edu.ua

Abstract: Our investigations show that electrochemical corrosion of copper is faster than electrochemical corrosion of aluminium at temperatures below 100°C. Literature data analysis shows that the Al atoms diffuse faster than the Cu atoms at temperatures higher than 475°C, Al rich intermetallic compounds (IMCs) are formed faster in the Cu-Al system, and the Kirkendall plane shifts toward Al side. Electrochemical corrosion occurs due to electric current and due to diffusion. An electronic devise working time, for example, depends on initial copper cover thickness on aluminium wire, connected to the electronic devise, temperature, and volume and dislocation pipe diffusion coefficients, so copper, iron, and aluminium electrochemical corrosion rates are investigated experimentally at room temperature and at temperature 100°C. Intrinsic diffusivities ratios of copper and aluminium at different temperatures and diffusion activation energies in the Cu-Al system are calculated by proposed here methods using literature experimental data. Dislocation pipe and volume diffusion activation energies of pure iron are calculated separately by earlier proposed method using literature experimental data. Aluminium dissolved into NaCl solution as the Al^{3+} ions at room temperature and at temperature 100°C, iron dissolved into NaCl solution as the Fe^{2+} (not Fe^{3+}) ions at room temperature and at temperature 100°C, copper dissolved into NaCl solution as the Cu^{+} ions at room temperature and as the Cu^{+} and the Cu^{2+} ions at temperature 100°C. It is founded experimentally that copper corrosion is higher than aluminium corrosion, and ratio of electrochemical corrosion rates, $k_{Cu}/k_{Al}>1$, decreases with temperature increasing, although iron electrochemical corrosion rate doesn't depend on temperature below 100°C. It is obvious, because melting point of iron is more higher then melting point of copper or aluminium. It is calculated that copper electrochemical corrosion rate is approximately equal to aluminium electrochemical corrosion at temperature about 300°C, so copper can dissolve into NaCl solution mostly as the Cu^{2+} ions at temperature about 300°C. Ratio of intrinsic diffusivities, $D_{Cu}/D_{Al}<1$, increases with temperature increasing, and intrinsic diffusivity of aluminium could be approximately equal to intrinsic diffusivity of copper at temperature about 460°C.

Keywords: electrochemical corrosion, metallic coatings, electrolysis, diffusion, intermetallic compounds, phases formation kinetics, copper, aluminium, iron, Kirkendall-Frenkel porosity, Kirkendall shift, activation energy

1. Introduction

An Al wire coated with thin Cu cover (≈15μm thickness), utilized near an automobile motor, is heated to temperatures about 373-473K (100-200°C). Intermetallics (IMCs) can formed at the Cu/Al interface and grow gradually during heating at such temperatures. The IMC layers are brittle and have high resistivity. Therefore, for assurance of the reliability of the product, information on the growth behaviour of the IMC layers during heating is essentially important [1]. Figure 1 shows the problem: an electronic devise working time, t_0, depends on initial Cu cover thickness, X_{Cu}, and temperature. Electric

Preprints (www.preprints.org) | NOT PEER-REVIEWED | Posted: 5 July 2021 doi:10.20944/preprints202107.0119.v1

conductivity of copper is higher than electric conductivity of aluminium in approximately two times, but the formation of intermetallic phases induce significant increase in contact resistance which is found to increase linearly with the thickness of the intermetallics formed [20]. The temperature range used to produce the intermetallic phases was from 250 to 515°C. Moreover, the presence of an electrical field greatly accelerated the kinetics of formation of intermetallic phases and altered significantly their morphology, and the impaired mechanical integrity of the Al-Cu bimetallic joints treated by an electrical current was clearly demonstrated by an extensive cracking not only across the whole intermetallic bandwidth but also within different phases and at a neighbouring interface [20]. Three phases thickness, X_{123}, can be estimated in such a way. The mass conservation law gives:

$$X_{Cu}(t=0)\cdot 1 = \frac{9}{9+4}X_3(t_0) + \frac{1}{1+1}X_2(t_0) + \frac{1}{1+2}X_3(t_0) \approx \frac{1.526\,X_{123}}{3} \approx 0.509\,X_{123}, \text{ and } X_{123} \approx 2\,X_{Cu}, \quad (1)$$

so three phases general thickness is approximately greater in two times than initial Cu cover thickness.

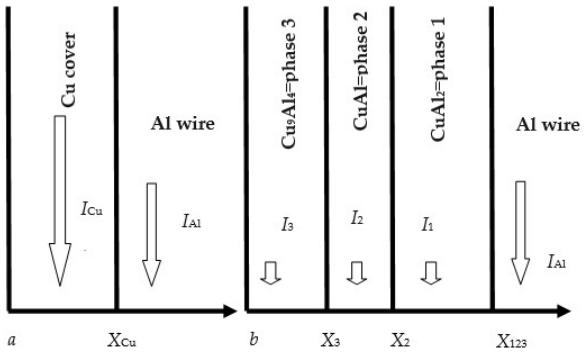

Figure 1. (*a*) Initial stage (t=0): an electronic devise is working, since the electric current, $I_a=I_{Cu}+I_{Al}$, has optimal value; (*b*) final stage ($t=t_0$): the electronic devise isn't working, because the electric current, $I_b=I_3+I_2+I_1+I_{Al}$, has too small value, since pure Cu cover has disappeared.

Otherwise, it was proved experimentally that thin Al pad (≈1 μm thickness) can prevent gold and copper corrosion, because intermetallics formation rate in Au-Al system is much more higher than intermetallics formation rate in Cu-Al system, so it is possible to use Cu instead of Au for wire bonding in microelectronics packaging, and Cu has higher electric conductivity, higher thermal conduction, and lower material cost than Au [2]. Corrosion and intermetallics rate formation in gold and copper wire bonding in microelectronics packaging were investigated in [2] at temperatures T_1=175 °C, T_2=200 °C, and T_3=225 °C during 120, 240, 360, and 480 h. The authors have reported that cross-sectional analysis of the Cu ball on Al pad confirmed that corrosion occurred at temperatures about T=200°C primarily beneath the Cu balls and did not initiate from the Al pad, formation of $CuCl_2$ didn't allow self-passivation of Cu to occur, so rate of copper corrosion increased, and the rate of Cu-Al intermetallics formation was found to be three to five times slower than Au-Al intermetallics formation at all three annealing temperatures. So, copper dissolved into NaCl solution as Cu^{2+} ions at temperatures about T=200°C, as we expected. They didn't investigate corrosion rates dependence of copper and aluminium on temperature. Moreover, phase layers general thicknesses for Cu-Al system were calculated [2]:

$$X_{123}^2 = K_{123}t + K_{01} = K_0 e^{-Q/(RT)} + K_{01} = 3.52\cdot 10^{-4}\ \mu m^2/s \cdot e^{-25500\ Jmol^{-1}/(RT)}t + 0.44\,\mu m^2, \quad (2)$$

Preprints (www.preprints.org) | NOT PEER-REVIEWED | Posted: 5 July 2021 doi:10.20944/preprints202107.0119.v1

where R≈8.314 JK^{-1} is the gas constant, K_{01} is constant related to initial IMC thickness. General reaction rates of IMC formation were calculated: $K_{123}(T_1)=3.57\cdot10^{-7}$ μm²/s, $K_{123}(T_2)=6.26\cdot10^{-7}$ μm²/s, and $K_{123}(T_3)=7.15\cdot10^{-7}$ μm²/s. The pre-exponential factor and IMC formation activation energy were calculated: $K_0\approx 3.52\cdot10^{-4}$ μm²/s, Q≈25.5 kJ/mol. We can use these results to calculate the electronic devise working time by equation (11) in [3] at different temperatures:

$$t_0 \approx \frac{X_{Cu}^2}{C_3^2 K_{123}} = \frac{169}{81}\frac{X_{Cu}^2}{K_{123}} \approx \frac{2X_{Cu}^2}{K_0} e^{Q/(RT)} \approx 5900 \cdot X_{Cu}^2[\mu m^2] \cdot e^{25.5 kJmol^{-1}/(RT)} s \quad (3)$$

$$t_0(T_1 = 175^o C = 448 K) \approx 5900 \cdot 225 \cdot e^{25500/(8.314\cdot 448)} s \approx 40 years \; ; \; t_0(T_2 = 200^o C) \approx 28 years \; ;$$

$$t_0(T_3 = 225^o C) \approx 21 years \; ; \quad t_0(T_4 = 300^o C) \approx 9 years \; ; \; t_0(T_5 = 350^o C) \approx 6 years \; .$$

Other researchers have obtained [15]: $K_{123}(T_4=300^oC)=4.2\cdot10^{-4}$ μm²/s, $K_{123}(T_5=350^oC)=3.4\cdot10^{-3}$ μm²/s. Equation (3) gives:

$$t_0(T_4 = 300^o C) \approx \frac{2X_{Cu}^2}{K_{123}} \approx 12 days \quad t_0(T_5 = 350^o C) \approx \frac{2X_{Cu}^2}{K_{123}} \approx 1.5 days \; ;$$

We can calculate: Q≈124 kJ/mol; $K_0\approx 8.5\cdot10^{-5}$ m²/s=$8.5\cdot10^{7}$ μm²/s;

$$t_0(T = 175^o C) \approx 5.3\cdot10^{-6} \cdot e^{124 Jmol^{-1}/(448 R)} s \approx 49 years \; ; \quad t_0(T = 200^o C) \approx 8.4 years \; ;$$

$$t_0(T = 225^o C) \approx \frac{2X_{Cu}^2}{K_0} e^{Q/(RT)} \approx 5.3\cdot10^{-6} \cdot e^{124 Jmol^{-1}/(498 R)} s \approx 1.7 years \; .$$

It was reported in [1] that the growth of layer 1 is controlled predominantly by boundary diffusion, but that of layers 2 and 3 are governed mainly by volume diffusion at temperatures T=483-543K (210-270°C) for various periods up to 3.456Ms (960h). The authors obtained: $K_{01}\approx 5.3\cdot10^{-7}$ m²/s, $Q_1\approx$86 kJ/mol, $K_{023}\approx 4.2\cdot10^{-5}$ m²/s, $Q_{23}\approx$146 kJ/mol. We can calculate: $K_{123}(T_6=210^oC)=1.5\cdot10^{-6}$ μm²/s,

$$t_0(T = 210^o C) \approx \frac{2X_{Cu}^2}{K_{123}} \approx 9.6 years \; .$$

The less temperature is, the higher contribution of grain-boundary diffusion and dislocation pipe diffusion to the layers growth is, so models of grain-boundary diffusion and dislocation pipe diffusion involving outflow into volume should be taken into account [11,17,19].

Diffusion activation energy of Al is less than diffusion activation energy of Cu ($Q_{Al}<Q_{Cu}$) at temperatures from 160°C to 250°C for mutual diffusion in copper–aluminium thin film double layers, but the pre-exponential factors are different in tens times [14]:

$$D_{Al}^* = 4\cdot10^{-5} e^{-121 kJmol^{-1}/(RT)} m^2/s \; , \quad D_{Cu}^* = 9.5\cdot10^{-4} e^{-135 kJmol^{-1}/(RT)} m^2/s \; , \quad (4)$$

in θ-phase (phase 1) $CuAl_2$, C_{Al}=2/3≈0.67, C_{Cu}=1/3≈0.33;

$$D_{Al}^* = 1.5\cdot10^{-11} e^{-68 kJmol^{-1}/(RT)} m^2/s \; , \quad D_{Cu}^* = 1\cdot10^{-6} e^{-106 kJmol^{-1}/(RT)} m^2/s \; , \quad (5)$$

 doi:10.20944/preprints202107.0119.v1

in η_2-phase (phase 2) CuAl, C_{Al}= C_{Cu}=1/2=0.5;

$$D_{Al}^{*} = 1.7 \cdot 10^{-7} e^{-116\,kJmol^{-1}/(RT)} m^2/s,\ D_{Cu}^{*} = 2.4 \cdot 10^{-6} e^{-125\,kJmol^{-1}/(RT)} m^2/s\ , \quad (6)$$

in γ_2-phase (phase 3) Cu_9Al_4, C_{Al}=4/13≈0.31, C_{Cu}=9/13≈0.69.

We can calculate mutual diffusion coefficient for each phase at temperature 160°C by the Darken equation [21,19] and taking into account Eqs. (4)-(6):

$$D_i^{*} = C_{Al} D_{Cu}^{*} + C_{Cu} D_{Al}^{*}; i = 1,2,3;\ \ D_1^{*} = 6.64 \cdot 10^{-20} m^2/s;\ D_2^{*} = 1.3 \cdot 10^{-19} m^2/s; D_3^{*} = 1.8 \cdot 10^{-21} m^2/s.$$

We can calculate using the methods described in [3,4]: $K_{123}(T_7$=160°C)≈2.8·10^{-6} μm^2/s, $t_0(T = 160^{o}C) \approx \frac{2X_{Cu}^{2}}{K_{123}} \approx 5\,years$, so the problem remains unsolved.

It was founded experimentally, that copper electrochemical corrosion is higher than aluminium electrochemical corrosion in approximately two times at room temperature [3,4], so thin Al layer can prevent copper electrochemical corrosion. It was reported also about influence of hydrogen and absence of passive layer on corrosive properties of aluminium alloys [5].

Besides, the soldered copper/tin based contacts are the weakest part of the chip that can be related to intermetallics and the Kirkendall-Frenkel porosity formation in the contact zone [6]. One of the most common reasons for chip failure is the soldered. The typical range of packaging and operation of the integrated circuits is from room temperature to 250°C [7].

Hydrostatic pressure of Argon gas (≈10 MPa) can decrease Kirkendal-Frenkel porosity formation, but practically can't decrease mutual diffusion coefficients, but hot isostatic pressing (p≈100 MPa, Argon) removes porosity due to homogenisation heat treatment in alloy CMSX4 and superalloy CMSX10 [8].

It was clarified also that carbon steel-stainless steel with the environment of flowing sodium chloride does indeed produce synergetic corrosion instead of antagonistic corrosion [9].

Electric current can destruct wire bonding in microelectronics packaging, so we planned to investigate copper, iron, and aluminium electrochemical corrosion at room temperature and at temperature 100°C. Direct current can dissolve metal anode into electrolyte, and we planned to do experiments under the same conditions: initial radii of Cu, Fe, and Al anodes should be approximately equal, electrolyte concentration should be the same, anodes lengths immersed into electrolyte should be equal, graphite cathodes should be the same, direct electric current value should be practically the same. Aluminium can dissolve into electrolyte only as the Al^{3+} ions, so the charge of aluminium ions should be exactly equal to 3, but copper can dissolve into electrolyte as the Cu^{+} ions and the Cu^{2+} ions, and the charge of copper ions could be equal to 1 or 2, and iron can dissolve into electrolyte as the Fe^{2+} ions and the Fe^{3+} ions, and the charge of iron ions could be equal to 2 or 3. We need to find appropriate mathematical equations to calculate the charges of copper, iron, and aluminium ions dissolved into NaCl solution.

2. Experimental results of copper, iron, and aluminium electrochemical corrosion

2.1. Investigation at room temperature

Cylindrical anodes (99.99 % Cu, 99.96 % Fe, and 99.99 % Al) were used for copper and aluminium [3,4], and also iron electrochemical corrosion investigation. Sodium chloride (NaCl) solution was used as electrolyte (Figure 2).

Preprints (www.preprints.org) | NOT PEER-REVIEWED | Posted: 5 July 2021 doi:10.20944/preprints202107.0119.v1

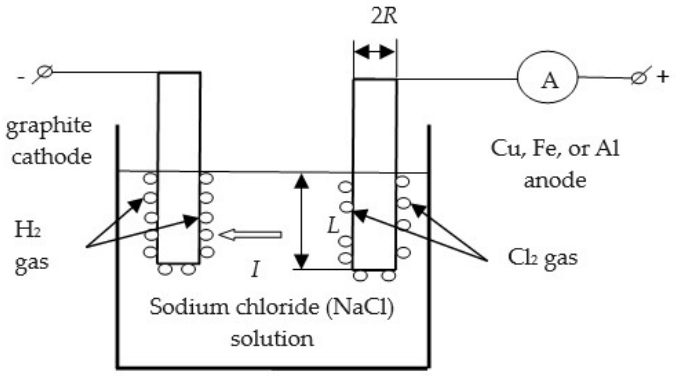

Figure 2. Scheme of experimental equipment at room temperature. Cu, Fe, and Al anodes dissolve into NaCl solution as Cu^{+}, Fe^{2+}, and Al^{3+} ions.

Direct electric current and anodes mass decreasing were measured. First of all, we need to be assured that the Cu^{+} ions (or the Cu^{2+}), the Fe^{2+} (or the Fe^{3+}), and the Al^{3+} were present in NaCl solution. Rate of anode dissolving into electrolyte can be calculated using Faraday's law of electrolysis:

$$\frac{dm}{dt} = \frac{MI}{zF}, \quad dm = \rho \cdot L \cdot \pi \cdot d(R^2(t)). \tag{4}$$

Here m is anode mass dissolved into electrolyte, t is time of experiment, M is molar mass, I is direct electric current value, F is the Faraday constant ($F \approx 96500\ C\ mol^{-1}$), z is charge of ions, R is anode radius, L is anode length immersed into electrolyte. Electric current value did not change, so one can calculate:

$$z = \frac{MIt}{F\pi\rho L(R^2(t=0) - R^2(t))}, \tag{5}$$

where ρ is anode density. Charges of copper, iron, and aluminium ions were calculated:

$$z_{Cu} = \frac{63.55 \cdot 10^{-3}\ {kg}/{mol} \cdot 2.8A \cdot 1.2 \cdot 10^3 s}{F \cdot \pi \cdot 8.9 \cdot 10^3\ {kg}/{m^3}\ L_{Cu} \cdot (R_{Cu}^2(t=0) - R_{Cu}^2(t_4))} \approx 0.995 \approx 1, \tag{6}$$

$$z_{Al} = \frac{27 \cdot 10^{-3}\ {kg}/{mol} \cdot 3.1A \cdot 1.2 \cdot 10^3 s}{F \cdot \pi \cdot 2.7 \cdot 10^3\ {kg}/{m^3}\ L_{Al} \cdot (R_{Al}^2(t=0) - R_{Al}^2(t_4))} \approx 2.954 \approx 3, \tag{7}$$

$$z_{Fe} = \frac{55.847 \cdot 10^{-3}\ {kg}/{mol} \cdot 3.15A \cdot 1.2 \cdot 10^3 s}{F \cdot \pi \cdot 7.86 \cdot 10^3\ {kg}/{m^3}\ L_{Fe} \cdot (R_{Fe}^2(t=0) - R_{Fe}^2(t_4))} \approx 2.03 \approx 2, \tag{8}$$

where $L_{Cu} \approx L_{Al} \approx L_{Fe}$: $L_{Cu} = L_{Fe} = 5 \cdot 10^{-2}$ m, $L_{Al} = 4.5 \cdot 10^{-2}$ m; $R_{0Cu} = R_{0Al} = 2.8$ mm, $R_{0Fe} = 2.98$ mm; $I_{Al} \approx I_{Cu} \approx I_{Fe}$: $I_{Fe} = 3.15$A, $I_{Al} = 3.1$A, $I_{Cu} = 2.8$A, so copper dissolved into NaCl solution as the Cu^{+} ions, iron dissolved into NaCl solution as the Fe^{2+} ions, and aluminium dissolved into NaCl solution as the Al^{3+} ions. Anodes radii decreasing kinetics is shown on Figure 2. Experiments were carried during t_1=5 min, t_2=10 min, t_3=15 min, and t_4=20 min.

Preprints (www.preprints.org) | NOT PEER-REVIEWED | Posted: 5 July 2021 doi:10.20944/preprints202107.0119.v1

Experimental results are as follows: R_{1Cu}=2.74 mm, R_{2Cu}=2.67 mm, R_{3Cu}=2.59 mm, R_{4Cu}=2.5 mm; R_{1Al}=2.77 mm, R_{2Al}=2.73 mm, R_{3Al}=2.68 mm, R_{4Al}=2.62 mm, R_{1Fe}=2.95 mm, R_{2Fe}=2.92 mm, R_{3Fe}=2.88 mm, R_{4Fe}=2.83 mm. Measurement precision was 0.01 mm or 10 micrometers.

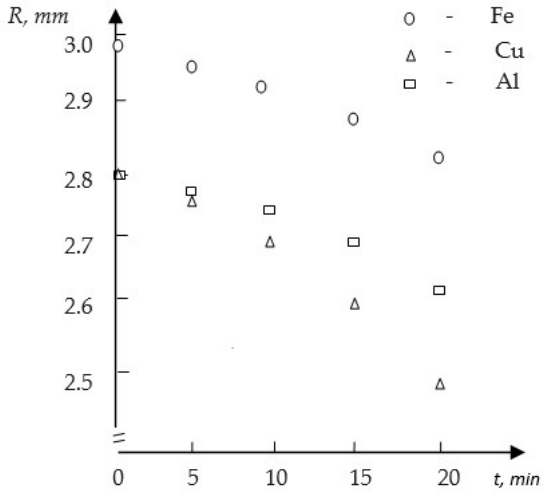

Figure 3. Cu, Fe, and Al anodes radii decreasing kinetics at room temperature.

Chemical reactions took place near positive electrode (anode):

$$Cu^0 - e^- = Cu^+, \quad Al^0 - 3e^- = Al^{3+}, \quad Fe^0 - 2e^- = Fe^{2+};$$

$$Cu^+ + Cl^- = CuCl\downarrow, Al^{3+} + 3Cl^- = AlCl_3\downarrow, \quad Fe^{2+} + 2Cl^- = FeCl_2\downarrow; \tag{9}$$

$$Cl^- - e^- = Cl^0, \; Cl^0 + Cl^0 = Cl_2\uparrow.$$

Chlorine gas was formed near anode.

Chemical reactions took place near negative electrode (cathode):

$$Na^+ - e^- = Na^0, \qquad 2Na + 2H_2O = 2NaOH + H_2\uparrow. \tag{10}$$

Hydrogen gas was formed near cathode.

Anodes radii decreasing rate constants can be calculated as average value of four experiments to increase calculation precise:

$$k_{Cu} = \frac{4R_0^2 - \sum_{i=1}^{4} R_i^2}{\sum_{i=1}^{4} t_i} \approx 1.25 \cdot 10^{-9}\, m^2/s, \quad k_{Al} = \frac{4R_0^2 - \sum_{i=1}^{4} R_i^2}{\sum_{i=1}^{4} t_i} \approx 7.29 \cdot 10^{-10}\, m^2/s, \tag{11}$$

$$k_{Fe} = \frac{4R_{0Fe}^2 - \sum_{i=1}^{4} R_{iFe}^2}{\sum_{i=1}^{4} t_i} \approx 7.26 \cdot 10^{-10}\, m^2/s, \quad k_{Cu} \approx 1.71 k_{Al}; k_{Al} \approx k_{Fe},$$

so copper electrochemical corrosion is much more higher than aluminium and iron electrochemical corrosion, despite of $I_{Fe} \approx I_{Al} \geq I_{Cu}$: $I_{Fe} \approx I_{Al} \approx 1.1 I_{Cu}$. It is need to point out that k_{Cu}, k_{Fe}, and k_{Al} have dimensionalities as diffusion coefficients [m²/s], because electrochemical corrosion occurs through anodes' surface.

Preprints (www.preprints.org) | NOT PEER-REVIEWED | Posted: 5 July 2021 doi:10.20944/preprints202107.0119.v1

2.2 Investigation at temperature 100 °C

Experiments were carried also at temperature 100°C. Cylindrical anodes (99.99 % Cu, 99.99 % Al, and 99.96 % Fe) were used for copper and aluminium [10], and also iron electric corrosion investigation. Sodium chloride (NaCl) solution was used as electrolyte (Figure 4). Direct electric current and anodes' mass decreasing rate were measured (Figure 5).

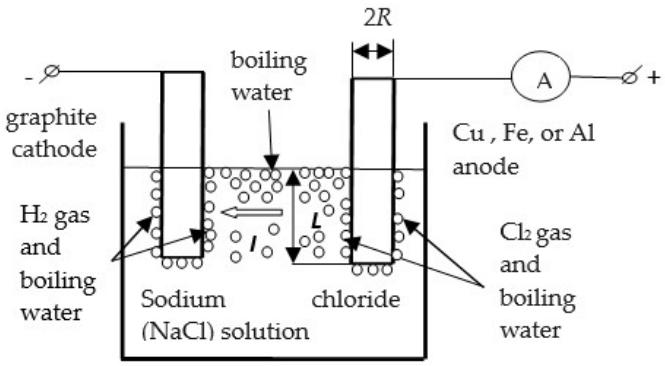

Figure 4. Scheme of experimental equipment at T=100°C. Cu, Fe, and Al anodes dissolve into NaCl solution as Cu^{+}, Cu^{2+}, Fe^{2+}, and Al^{3+} ions.

Electric current value did not change, so one can calculate:

$$z_{Cu} = \frac{63.55 \cdot 10^{-3}\, kg/mol \cdot 3.05\, A \cdot 1.2 \cdot 10^{3}\, s}{F \cdot \pi \cdot 8.9 \cdot 10^{3}\, kg/m^{3} \cdot L_{Cu} \cdot (R_{Cu}^{2}(t=0) - R_{Cu}^{2}(t_4))} \approx 1.47 \approx \frac{1+2}{2}, \quad (12)$$

$$z_{Al} = \frac{27 \cdot 10^{-3}\, kg/mol \cdot 3.15\, A \cdot 1.2 \cdot 10^{3}\, s}{F \cdot \pi \cdot 2.7 \cdot 10^{3}\, kg/m^{3} \cdot L_{Al} \cdot (R_{Al}^{2}(t=0) - R_{Al}^{2}(t_4))} \approx 2.85 \approx 3, \quad (13)$$

$$z_{Fe} = \frac{55.847 \cdot 10^{-3}\, kg/mol \cdot 3.15\, A \cdot 1.2 \cdot 10^{3}\, s}{F \cdot \pi \cdot 7.86 \cdot 10^{3}\, kg/m^{3} \cdot L_{Fe} \cdot (R_{Fe}^{2}(t=0) - R_{Fe}^{2}(t_4))} \approx 2.01 \approx 2, \quad (14)$$

where L_{Cu}=L_{Al}=4·10^{-2} m, L_{Fe}=5·10^{-2} m, R_{0Cu}=2.27 mm, R_{0Al}=2.6 mm, R_{0Fe}=2.83 mm, I_{Al} =3.15 A, I_{Fe} =3.13 A, I_{Cu} =3.05 A, so copper dissolved into NaCl solution as Cu^{+} and Cu^{2+} ions (copper dissolved into NaCl solution as Cu^{+} ions at room temperature), iron dissolved into NaCl solution as the Fe^{2+} ions (as at room temperature), and aluminium dissolved into NaCl solution as Al^{3+} ions (as at room temperature). Anodes radii decreasing kinetics is shown on Figure 5. Experiments were carried during t_1=5 min, t_2=10 min, t_3=15 min, and t_4=20 min. Experimental results are as follows: R_{1Cu}=2.2 mm, R_{2Cu}=2.12 mm, R_{3Cu}=2.03 mm, R_{4Cu}=1.92 mm; R_{1Al}=2.56 mm, R_{2Al}=2.51 mm, R_{3Al}=2.45 mm, R_{4Al}=2.38 mm; R_{1Fe}=2.80 mm, R_{2Fe}=2.76 mm, R_{3Fe}=2.72 mm, R_{4Fe}=2.67 mm. Measurement precision was 0.01 mm or 10 micrometers. We carried additional experiments, but result was the same.

Chemical reactions are more complicated at 100°C than at room temperature near positive electrodes (anodes):

$$Cu^{0} - e^{-} = Cu^{+},\ Cu^{0} - 2e^{-} = Cu^{2+},\quad Al^{0} - 3e^{-} = Al^{3+},\quad Fe^{0} - 2e^{-} = Fe^{2+};$$

$$Cu^{+} + Cl^{-} = CuCl\downarrow,\ Al^{3+} + 3Cl^{-} = AlCl_3\downarrow,\quad Fe^{2+} + 2Cl^{-} = FeCl_2\downarrow; \quad (15)$$

Preprints (www.preprints.org) | NOT PEER-REVIEWED | Posted: 5 July 2021 doi:10.20944/preprints202107.0119.v1

$$Cu^{2+} + 2Cl^- = CuCl_2 \downarrow, Cl^- - e^- = Cl^0,\ Cl^0 + Cl^0 = Cl_2 \uparrow.$$

Chlorine gas and boiling water were formed near anodes.

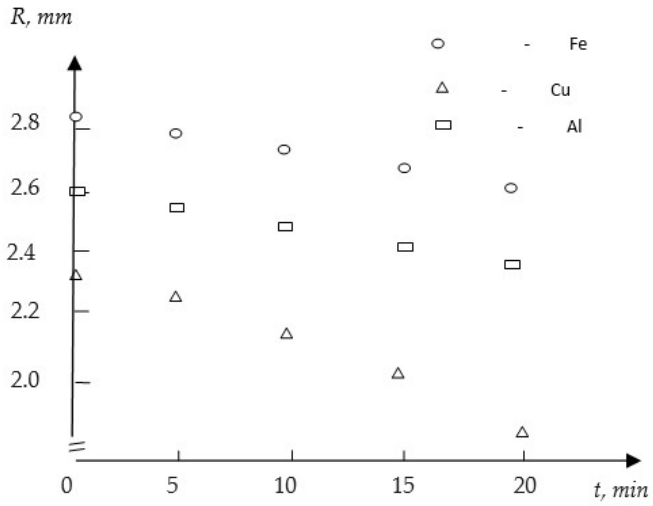

Figure 5. Cu, Fe, and Al anodes radii decreasing kinetics at T=100°C.

Chemical reactions took place near negative electrodes (cathodes):

$$Na^+ - e^- = Na^0,\ 2Na + 2H_2O = 2NaOH + H_2 \uparrow. \quad (16)$$

Hydrogen gas and boiling water were formed near cathodes.

Anodes radii decreasing rate constants can be calculated as average value of four experiments to increase calculation precise:

$$k_{Cu} = \frac{4R_{0Cu}^2 - \sum_{i=1}^{4} R_{iCu}^2}{\sum_{i=1}^{4} t_i} \approx 1.154 \cdot 10^{-9}\, m^2/s,\ \{1.25 \cdot 10^{-9} \text{ at room temperature}\},$$

$$k_{Al} = \frac{4R_{0Al}^2 - \sum_{i=1}^{4} R_{iAl}^2}{\sum_{i=1}^{4} t_i} \approx 8.42 \cdot 10^{-10}\, m^2/s,\ \{7.29 \cdot 10^{-10} \text{ at room temperatur} \quad (17)$$

$$k_{Fe} = \frac{4R_{0Fe}^2 - \sum_{i=1}^{4} R_{iFe}^2}{\sum_{i=1}^{4} t_i} \approx 6.83 \cdot 10^{-10}\, m^2/s,\ \{7.23 \cdot 10^{-10} \text{ at room temperature}\}, k_{Cu} \approx 1.37 k_{Al},\ \{1.72 \text{ at room temperature}$$

$T_1 \approx 27$°C},

so copper electrochemical corrosion is higher at room temperature T_1≈27°C, aluminium electrochemical corrosion is higher at temperature T_2=100°C, and ratio of electrochemical corrosion rates, k_{Cu}/k_{Al}, decreases with temperature increasing, although iron electrochemical corrosion rate practically doesn't depend on temperature below 100°C. It is obvious, because of higher melting point of iron than melting point of copper or aluminium. We

Preprints (www.preprints.org) | NOT PEER-REVIEWED | Posted: 5 July 2021 doi:10.20944/preprints202107.0119.v1

can conclude that the Cu^{2+} ions are less mobile than Cu^{+} ions. It is need to point out that k_{Cu}, k_{Al}, and k_{Fe} have dimensionalities as diffusion coefficients, D^*_{Cu}, D^*_{Al}, D^*_{Fe} [m²/s], because electrochemical corrosion occurs through anodes' surface.

Dislocation pipe and volume diffusion activation energies can be calculated in such a way. The Arrhenius law is valid for dislocation pipe diffusion and volume diffusion in ultra high purity samples [11,19]:

$$D^*_d = D_{0d}e^{-Q_d/(RT)} \text{ or } D^*_d = D_{0d}e^{-E_d/(k_BT)}, \text{ and } D^*_V = D_{0V}e^{-Q_V/(RT)} \text{ or } D^*_V = D_{0V}e^{-E_V/(k_BT)}, \quad (18)$$

$$Q[J/mol] = F \cdot E[eV]. \quad (19)$$

Here R≈8.314 JK^{-1} is the gas constant, k_B is the Boltzmann constant, $Q_d(E_d)$ is the dislocation pipe diffusion activation energy ($Q_d=FE_d$), $F \approx 96500\ Cmol^{-1}$ is the Faraday constant, $Q_V(E_V)$ is the volume diffusion activation energy ($Q_V=FE_V$), D_{0d} and D_{0V} are the pre-exponential factors, T is absolute temperature.

Our experimental results allow to calculate:

$$\frac{k_{Cu}}{k_{Al}}(T) \approx \frac{D^*_{Cu}}{D^*_{Al}}(T) = \frac{D^*_{0Cu}}{D^*_{0Al}}e^{(Q_{Al}-Q_{Cu})/(RT)}; \ln\left(\frac{D^*_{0Cu}}{D^*_{0Al}}\right) = -0.6; Q_{Al} - Q_{Cu} = 2.9kJ/mol, \quad (20)$$

$$\frac{D^*_{0Cu}}{D^*_{0Al}} = 0.55, \quad \frac{D^*_{Cu}}{D^*_{Al}}(T_3) = 1 \Rightarrow T_3 = \frac{2900\ J/mol}{0.6R} \approx 583\ K \approx 310^oC, \quad (21)$$

so diffusion activation energy of Al, Q_{Al}, is higher than diffusion activation energy of Cu, Q_{Cu}, ($Q_{Al}>Q_{Cu}$, Q_{Al}-Q_{Cu} = 2.9 kJ / mol), at temperatures from 20°C to 100°C, because the Cu^{+} ions have higher mobilities than the Al^{3+} ions, and copper electrochemical corrosion rate can be approximately equal to aluminium electrochemical corrosion at temperature about T_3≈300°C due to the Cu^{2+} ions are less mobile than the Cu^{+} ions. Moreover, the pre-exponential factors are approximately the same: D^*_{0Al}≈$2D^*_{0Cu}$.

3. Intrinsic diffusivities ratio and diffusion activation energy calculations

3.1. Intrinsic diffusivities ratio of Cu and Al analysis

We can analyse described experimental results in the Al-Cu system for bulk samples [12], since the ratio D^*_{Al}/D^*_{Cu} didn't calculated in [12]:

$$\frac{D^*_{Cu}}{D^*_{Al}} \approx \frac{\sum_{j=1}^{N} X_j - X_K(1-C_i)\sqrt{\pi}}{\sum_{j=1}^{N} X_j + C_i X_K \sqrt{\pi}} < 1, \quad C_i = C_{Al}, \quad (22)$$

where N is formed phases quantity, X_j is phase j's thickness, C_i is is the average concentration of aluminium in phase i, X_K is the Kirkendall shift length.

Five phases are formed in the Al-Cu system at temperatures from 400°C to 535°C in bulk samples [12]: θ-phase (phase 1) $CuAl_2$ (C_1=2/3), η₂-phase (phase 2) CuAl (C_2=1/2), ζ₂-phase (phase 3b) Cu_4Al_3 (C_{3b}=3/7), δ-phase (phase 3a) Cu_3Al_2 (C_{3a}=2/5), and γ₂-phase (phase 3) Cu_9Al_4 (C_3=4/13≈0.31≈1/3, C=C_{Al}). Inert markers were in δ-phase (phase 3a) Cu_3Al_2 (C_{3a}=2/5=0.4) and moved to Al side during mutual diffusion. In general, inert markers move to faster diffusivity component side. We can calculate (C_{3a}=0.4):

$$\frac{D^*_{Cu}}{D^*_{Al}}(T_1 = 535^oC) \approx \frac{X_1 + X_2 + X_{3b} + X_{3a} + X_3 - X_K 0.6\sqrt{\pi}}{X_1 + X_2 + X_{3b} + X_{3a} + X_3 + 0.4X_K\sqrt{\pi}} \approx 0.814; y_1 = \frac{D^*_{Al}}{D^*_{Cu}} = \frac{1}{0.814} \approx 1.228, \quad (23)$$

T_1=535°C=808K, t=40h, X_K≈20.5μm, X_1+X_2+X_{3b}+X_{3a}+X_3≈180μm;

$$\frac{D^*_{Cu}}{D^*_{Al}}(T_2 = 515^oC) \approx \frac{X_1 + X_2 + X_{3b} + X_{3a} + X_3 - X_K(1-C_{3a})\sqrt{\pi}}{X_1 + X_2 + X_{3b} + X_{3a} + X_3 + C_{3a}X_K\sqrt{\pi}} \approx 0.856; y_2 = \frac{D^*_{Al}}{D^*_{Cu}} \approx 1.168, \quad (24)$$

Preprints (www.preprints.org) | NOT PEER-REVIEWED | Posted: 5 July 2021 doi:10.20944/preprints202107.0119.v1

T_2=515 °C =788K, t=40h, X_K≈11μm, $X_1+X_2+X_{3b}+X_{3a}+X_3$≈127μm);

$$\frac{D^*_{Cu}}{D^*_{Al}}(T_3 = 495^oC) \approx \frac{X_1 + X_2 + X_{3b} + X_{3a} + X_3 - X_K\, 0.6\sqrt{\pi}}{X_1 + X_2 + X_{3b} + X_{3a} + X_3 + 0.4X_K\sqrt{\pi}} \approx 0.916; y_3 = \frac{1}{0.916} \approx 1.092\,, \quad (25)$$

T_3=495 °C =768K, t=40h, X_K ≈5μm, $X_1+X_2+X_{3b}+X_{3a}+X_3$≈ 101μm;

$$\frac{D^*_{Cu}}{D^*_{Al}}(T_4 = 475^oC) \approx \frac{X_1 + X_2 + X_{3b} + X_{3a} + X_3 - X_K(1-0.4)\sqrt{\pi}}{X_1 + X_2 + X_{3b} + X_{3a} + X_3 + 0.4CX_K\sqrt{\pi}} \approx 0.969; y_4 = \frac{D^*_{Al}}{D^*_{Cu}} \approx 1.032\,, \quad (26)$$

T_4=475°C=748K, t=90h, X_K≈2μm, $X_1+X_2+X_{3b}+X_{3a}+X_3$≈113μm.

We can use these four points to calculate by the least square method to increase calculation precise:

$$\Delta Q = Q_{Al} - Q_{Cu} = \frac{4\sum_{j=1}^{4}\left(\frac{1000}{RT_j}\ln y_j\right) - \sum_{j=1}^{4}\ln y_j \sum_{j=1}^{4}\frac{1000}{RT_j}}{4\sum_{j=1}^{4}\left(\frac{1000}{RT_j}\right)^2 - \left(\sum_{j=1}^{4}\frac{1000}{RT_j}\right)^2} \approx -13.4 kJ/mol\,, \quad (27)$$

$$y_0 = \exp\frac{\sum_{j=1}^{4}\left(\frac{1000}{RT_j}\right)^2 \sum_{j=1}^{4}\ln y_j - \sum_{j=1}^{4}\frac{1000}{RT_j}\sum_{j=1}^{4}\left(\frac{1000}{RT_j}\ln y_j\right)}{4\sum_{j=1}^{4}\left(\frac{1000}{RT_j}\right)^2 - \left(\sum_{j=1}^{4}\frac{1000}{RT_j}\right)^2} \approx \exp(2.2) \approx 9\,, \quad (28)$$

$$\frac{D^*_{Al}}{D^*_{Cu}}(T) = \frac{D^*_{0Al}}{D^*_{0Cu}} e^{(Q_{Al}-Q_{Cu})/(RT)} \approx 9e^{-13.4 kJmol^{-1}/(RT)}, \quad (29)$$

$$\frac{D^*_{Al}}{D^*_{Cu}}(T_5) = y_5 = 1 \Rightarrow T_5 = \frac{13400\ J/mol}{R\ln 9} \approx 733\ K \approx 460^oC\,, \quad (30)$$

so Q_{Al}<Q_{Cu} (Q_{Al}-Q_{Cu}=-13.4kJ/mol) because the Cu^{2+} ions have less mobilities than the Al^{3+} ions, and we can conclude that the Kirkendall displacement changes sign at temperature about T_5≈460°C for bulk samples. The pre-exponential factors are different in nine times: D^*_{0Al}≈9D^*_{0Cu}.

Diffusion activation energy of Al is less than diffusion activation energy of Cu (Q_{Al}<Q_{Cu}) at temperatures from 160°C to 250°C for mutual diffusion in copper–aluminium thin film double layers, but the pre-exponential factors are different in tens times [14]. Isolated W islands, 150 Å in diameter, have been deposited between Cu and Al thin film double layers to serve as inert diffusion markers. Marker displacements have been measured. We can calculate ratio D^*_{Al}/D^*_{Cu} for each phase at different temperatures:

$$\frac{D^*_{Cu}}{D^*_{Al}}(T) = \frac{D^*_{0Cu}}{D^*_{0Al}} e^{(Q_{Al}-Q_{Cu})/(RT)} = 24e^{-14 kJmol^{-1}/(RT)}$$ in θ-phase (phase 1) $CuAl_2$, C_{Al}=2/3≈0.67,

$$\frac{D^*_{1Cu}}{D^*_{1Al}}(T = 250^oC = 523\,K) = 24e^{-14000\ Jmol^{-1}/(8.314\,x523)} \approx 24e^{-3.22} \approx 0.96\,,$$

$$\frac{D^*_{1Cu}}{D^*_{1Al}}(T = 160^oC = 433\,K) \approx 24e^{-3.89} \approx 0.49\,,$$

Preprints (www.preprints.org) | NOT PEER-REVIEWED | Posted: 5 July 2021 doi:10.20944/preprints202107.0119.v1

so the Al atoms diffuse faster than the Cu atoms in θ-phase at temperatures from 160°C to 250°C;

$\frac{D^*_{Cu}}{D^*_{Al}}(T)=\frac{D^*_{0Cu}}{D^*_{0Al}}e^{(Q_{Al}-Q_{Cu})/(RT)}=7\cdot10^4 e^{-38\,kJmol^{-1}/(RT)}$ in η_2-phase (phase 2) CuAl, C_{Al}=1/2=0.5,

$\frac{D^*_{2Cu}}{D^*_{2Al}}(T=250^oC)=7\cdot10^4 e^{-38000\,Jmol^{-1}/(RT)}\approx11.2$, $\frac{D^*_{2Cu}}{D^*_{2Al}}(T=160^oC)\approx1.8$,

so the Cu atoms diffuse faster than the Al atoms in η_2-phase at temperatures from 160°C to 250°C;

$\frac{D^*_{Cu}}{D^*_{Al}}(T)=\frac{D^*_{0Cu}}{D^*_{0Al}}e^{(Q_{Al}-Q_{Cu})/(RT)}=14e^{-9\,kJmol^{-1}/(RT)}$ in γ_2-phase (phase 3) Cu_9Al_4, C_{Al}=4/13≈0.31,

$\frac{D^*_{3Cu}}{D^*_{3Al}}(T=250^oC)=14e^{-9000\,Jmol^{-1}/(RT)}\approx1.77$, $\frac{D^*_{3Cu}}{D^*_{3Al}}(T=160^oC)=14e^{-9\,kJmol^{-1}/(RT)}\approx1.15$,

so the Cu atoms diffuse faster than the Al atoms in γ_2-phase at temperatures from 160°C to 250°C.

The Cu rich phases can be formed faster than the Al rich phases at temperatures from 160°C to 250°C, and the Cu atoms can diffuse faster than the Al atoms in the Al-Cu system at temperatures from 160°C to 250°C. The Al rich phases can be formed faster than the Cu rich phases at temperatures from 400°C to 535°C, and the Al atoms can diffuse faster than the Cu atoms in the Al-Cu system at temperatures from 400°C to 535°C. It depends on the crystal structure of each phase, but, in general, it could depends on conclusions that the Cu^{2+} ions are less mobile than the Cu+ ions, and the ratio D^*_{Al}/D^*_{Cu} depends on temperature.

3.2. Diffusion activation energy calculation

3.2.1 Diffusion activation energy calculation in the Cu-Al system

Mutual diffusion coefficients were calculated for all five phases [12]:

$$\tilde{D}^*_1=5.6\cdot10^{-5}e^{-127.6\,kJmol^{-1}/(RT)}m^2/s;\ \tilde{D}^*_2=2.2\cdot10^{-4}e^{-148.5\,kJmol^{-1}/(RT)}m^2/s; \quad (31)$$

$\tilde{D}^*_{3b}=1.6\cdot10^2 e^{-230.5\,kJmol^{-1}/(RT)}m^2/s$, $\tilde{D}^*_{3a}=2.1\cdot10^{-4}e^{-138.1\,kJmol^{-1}/(RT)}m^2/s$, $\tilde{D}^*_3=8.5\cdot10^{-5}e^{-136\,kJmol^{-1}/(RT)}m^2/s$.

We can see that $Q_1<Q_2$, $Q_1<Q_3$, and $Q_3<Q_2$ because of $K_1>K_2$, $K_1>K_3$, and $K_3>K_2$, and $D_{01}\approx D_{02}\approx D_{03}$. Phase j's rate formation is K_j. Three phases are formed in the Al-Cu system at temperatures 300°C and 350°C [15]: $CuAl_2$, CuAl, and Cu_9Al_4. Phases formation rates were experimentally measured: K_1=860x10^{-18} m^2/s, K_2=100x10^{-18} m^2/s, and K_3=360x10^{-18} m^2/s at temperature 350°C; K_1=77x10^{-18} m^2/s, K_2=18x10^{-18} m^2/s, and K_3=35x10^{-18} m^2/s at temperature 300°C, so $K_1>K_2$, $K_1>K_3$, and $K_3>K_2$. We can calculate assuming C_1=2/3, C_2=1/2, C_3=1/3, $C=C_{Al}$ [4]:

$$D_1\approx\frac{1}{2}(C_1(1-C_1)K_1+C_2(1-C_1)\sqrt{K_1K_2}+C_3(1-C_1)\sqrt{K_1K_3}); \quad (32)$$

$$D_2\approx\frac{1}{2}(C_2(1-C_2)K_2+C_2(1-C_1)\sqrt{K_1K_2}+C_3(1-C_2)\sqrt{K_2K_3}); \quad (33)$$

Preprints (www.preprints.org) | NOT PEER-REVIEWED | Posted: 5 July 2021 doi:10.20944/preprints202107.0119.v1

$$D_3 \approx \frac{1}{2}(C_3(1-C_3)K_3 + C_3(1-C_1)\sqrt{K_1K_3} + C_3(1-C_2)\sqrt{K_2K_3}); \quad (34)$$

$$D_1(T_2 = 350\,^0C) \approx \frac{1}{9}K_1 + \frac{1}{12}\sqrt{K_1K_2} + \frac{1}{18}\sqrt{K_1K_3} \approx 150\cdot10^{-18}\,m^2/s\,, D_1(T_1 = 300\,^oC) \approx 15\cdot10^{-18}\,m^2/s\,; \quad (35)$$

$$D_2(T_2 = 350^oC) \approx \frac{1}{8}K_2 + \frac{1}{12}\sqrt{K_1K_2} + \frac{1}{12}\sqrt{K_2K_3} \approx 50x10^{-18}\,m^2/s\,, \quad D_2(T_1 = 300\,^oC) \approx 8\cdot10^{-18}\,m^2/s\,; \quad (36)$$

$$D_3(T_2 = 350^oC) \approx \frac{1}{9}K_3 + \frac{1}{18}\sqrt{K_1K_3} + \frac{1}{12}\sqrt{K_2K_3} \approx 90\cdot10^{-18}\,m^2/s\,, \quad D_3(T_1 = 300\,^oC) \approx 12\cdot10^{-18}\,m^2/s\,. \quad (37)$$

Authors [15] didn't calculate diffusion activation energies and the pre-exponential factors, so we can do it:

$$Q_i = \frac{RT_1T_2}{T_2 - T_1}\ln\left(\frac{D_i(T_2)}{D_i(T_1)}\right), \qquad D_{0i} = D_i(T_1)e^{Q_i/(RT_1)} = D_i(T_2)e^{Q_i/(RT_2)}; \quad (38)$$

$$\widetilde{D}_1 = 4.3\cdot10^{-5}e^{-136.7kJmol^{-1}/(RT)}m^2/s\,, \quad \widetilde{D}_2 = 6.6\cdot10^{-8}e^{-108.8kJmol^{-1}/(RT)}m^2/s\,, \quad (39)$$

$$\widetilde{D}_3 = 9.6\cdot10^{-7}e^{-119.6kJmol^{-1}/(RT)}m^2/s\,.$$

Equations (39) correspond to Equations (31). We can use several, N, points to calculate by the least square method to increase calculation precise:

$$Q_i = -\frac{N\sum_{j=1}^{N}\left(\frac{1000}{RT_j}\ln D_i(T_j)\right) - \sum_{j=1}^{N}\ln D_i(T_j)\sum_{j=1}^{N}\frac{1000}{RT_j}}{N\sum_{j=1}^{N}\left(\frac{1000}{RT_j}\right)^2 - \left(\sum_{j=1}^{N}\frac{1000}{RT_j}\right)^2}[kJ/mol]\,, \quad (40)$$

$$D_{0i} = \exp\frac{\sum_{j=1}^{5}\left(\frac{1000}{RT_j}\right)^2\sum_{j=1}^{5}\ln D_i(T_j) - \sum_{j=1}^{5}\frac{1000}{RT_j}\sum_{j=1}^{4}\left(\frac{1000}{RT_j}\ln D_i(T_j)\right)}{5\sum_{j=1}^{5}\left(\frac{1000}{RT_j}\right)^2 - \left(\sum_{j=1}^{5}\frac{1000}{RT_j}\right)^2}[m^2/s]\,. \quad (41)$$

Equations (40) and (41) give Equations (38) for only two points (N=2).

3.2.2. Diffusion activation energy calculation in pure iron

A method of dislocation pipe diffusion parameters determination during the type B diffusion kinetics was suggested by model of dislocation pipe diffusion involving outflow [11]. The method involves diffusion dislocation pipe kinetics for two different annealing times at the same temperature during the type B kinetics and dislocation pipe kinetics for one annealing time at other lower temperature during the type C kinetics. Transition time for type B kinetics to type A kinetics (volume diffusion) and kinetics law $t^{1/6}$ [17] for cone top rate are used in this method.

Bulk diffusion coefficients, D_V, for the diffusion of ^{59}Fe in the high purity iron were calculated in [16] using type B→A kinetics: D_V=1.5*10^{-18} m^{2}s^{-1} at T_1=973K for $t_{B\to A}$=67.5ks (T_m/T_1=1.86, T_m is melting point of iron). Only one experiment was carried out at the same

temperature for two annealing times t_1 and t_2 ($t_1 << t_2$, $t_2 = 40\ t_1$). Dislocation diffusion coefficients for the diffusion of ^{59}Fe in the iron were calculated in [16] using type C kinetics: $D_d = 3*10^{-16}$ m^{2}s^{-1} at $T_2 = 753$K for $t_C = 2.4$ks ($T_m/T_2 = 2.4$). One can find ratio D_d/D_V: $y(t_{C\to B}) = \sqrt{\frac{D_d}{6D}\delta}$, where $\delta = 1$ nm, $\frac{D_d}{D} = 4.3x10^6$. Ratio D_d/D_V increases remarkably for lower temperature. Dislocation pipe and volume diffusion activation energies and pre-exponential factors didn't were calculated in [16]. It is possible to calculate E_d and D_0: $E_d = \ln\left(\frac{D_d(T_1)}{D_d(T_2)}\right)k_B\frac{T_1T_2}{T_1 - T_2}$, $D_0 = D_d(T_1)\exp\left(\frac{E_d}{k_BT_1}\right)$, $E_d = 1.1eV; Q_d = 106kJ/mol$, $D_0 = 6.85\cdot10^{-9}m^2s^{-1}$. One can calculate dislocation pipe diffusion coefficient for temperature973 K directly ($T_1 = 753$ K and $T_2 = 693$ K (type C kinetics)): $D_d \approx 10^{-14}$ m^{2}s^{-1}. Such value corresponds to value calculated using proposed method. The Fisher law ($t^{1/4}$) gives: $D_d \approx 10^{-16} \div 10^{-15}$ m^{2}s^{-1}. Such value is in two orders lower than experimentally obtained in [16]. The volume diffusion activation energy E_V can be calculated: $E_V = \ln\left(\frac{D_0}{D_V(T_1)}\right)k_BT_1$, $E_V = 1.85eV; Q_V \approx 179kJ/mol$. Ratio $\frac{E_d}{E_V} = 0.6$ as described in [19].

4. Conclusions

The Al atoms diffuse faster than the Cu atoms at temperature higher than 475°C, but the Cu atoms diffuse faster than the Al atoms at temperature lower than 100°C. Diffusion activation energy of Al is less than diffusion activation energy of Cu at temperature higher than 475°C, but diffusion activation energy of Cu is less than diffusion activation energy of Al at temperature lower than 100°C. Our investigations show that it is possible, because the Cu^{2+} ions are less mobile than Cu^{+} ions.

Volume diffusion activation energy of Fe is higher that volume diffusion activation energy of Cu or Al, but dislocation pipe diffusion activation energy of Fe is smaller that volume diffusion activation energy of Cu or Al, so the Fe atoms diffuse faster along dislocation line, but the Cu or Al atoms diffuse faster in volume.

References

1. Kizaki T, O M, Kajihara M. Rate-Controlling Process of Compound Growth in Cu-Clad Al Wire during Isothermal Annealing at 483–543 K. Materials Transactions. 2020;61(1):188-194. DOI: https://10.2320/matertrans.MT-M2019207
2. Goh CS, Chong W L E, Lee TK, Breach C. Corrosion Study and Intermetallics Formation in Gold and Copper Wire Bonding in Microelectronics Packaging. Crystals. 2013;3(3):391-404. DOI: https://doi.org/10.3390/cryst3030391
3. Yarmolenko MV. Copper and aluminum electric corrosion investigation and intermetallics disappearance in Cu-Al system analysis. Phys. Chem. Solid St. 2020;21(2):294-299. https://journals.pnu.edu.ua/index.php/pcss/article/view/3055
4. Yarmolenko MV. Intermetallics Disappearance Rate Analysis in Double Multiphase Systems. DDF. 2021;407:68–86. https://doi.org/10.4028/www.scientific.net/ddf.407.68
5. Włodarczyk PP, Włodarczyk B. Effect of Hydrogen and Absence of Passive Layer on Corrosive Properties of Aluminium Alloys. Materials. 2020; 13(7): 1580-1593. https://doi.org/10.3390/ma13071580
6. Kumar S, Handwerker CA, Dayananda MA. Intrinsic and Interdiffusion in Cu-Sn System. JPEDAV. 2011;32:309-319. DOI: 10.1007/s11669-011-9907-91547-7037
7. Tu KN. Electronic Thin-Film Reliability. 1st ed. Cambridge University Press: New York; 2010. 392 p. DOI: https://www.amazon.com/Electronic-Thin-Film-Reliability-King-Ning-Tu-ebook-dp-B00QIT3LXA/dp/B00QIT3LXA/ref=mt_other?_encoding=UTF8&me=&qid=
8. Epishin A, Chyrkin A, Camin B, Saillard R, Gouy S, Viguier B. Interdiffusion in CMSX-4 Related Ni-Base Alloy System at a Supersolvus Temperature. DDF. 2021;407:1–10. https://doi.org/10.4028/www.scientific.net/ddf.407.1
9. Prawoto Y. Synergy of erosion and galvanic effects of dissimilar steel welding: Field failure analysis case study and laboratory test results. Journal of King Saud University – Engineering Sciences. 2013;25:59–64. https://doi.org/10.1016/j.jksues.2011.12.001
10. Yarmolenko MV. Intrinsic Diffusivities Ratio Analysis in the Al-Cu System. Phys. Chem. Solid St. 2020;21(4):720-726. https://journals.pnu.edu.ua/index.php/pcss/article/view/4440
11. Yarmolenko MV. Method of Dislocation and Bulk Diffusion Parameters Determination. Metallofiz. Noveishie Tekhnol.. 2020;42(11): 1537–1546. https://mfint.imp.kiev.ua/article/v42/i11/MFiNT.42.1537.pdf

12. Funamizu Y, Watanabe K. Interdiffusion in the Al–Cu System. Transactions of the Japan Institute of Metals. 1971;12(3):147-152. 10.2320/matertrans1960.12.147
13. Yarmolenko MV. Intermetallics Disappearance Rates and Intrinsic Diffusivities Ratios Analysis in the Cu-Zn and the Cu-Sn Systems. Phys. Chem. Solid St. 2021;22(1):80-87. https://journals.pnu.edu.ua/index.php/pcss/article/view/4744
14. Hentzell HTG, Tu KN. Interdiffusion in copper–aluminum thin film bilayers. II. Analysis of marker motion during sequential compound formation. Journal of Applied Physics. 1983;54:6929-6937. https://doi.org/10.1063/1.332000
15. Moisy F, Sauvage X, Hug E. Investigation of the early stage of reactive interdiffusion in the Cu-Al system by *in-situ* transmission electron microscopy. Materialia. 2020;9: 100633. https://doi.org/10.1016/j.mtla.2020.100633
16. Shima Y, Ishikawa Y, Nitta H, Yamazaki Y, Mimura K, Isshiki M, Iijima Y. Self-Diffusion along Dislocations in Ultra High Purity Iron. Materials Transactions. 2002;43(2): 173-177. https://www.jim.or.jp/journal/e/43/02/173.html
17. Yarmolenko MV. Intermediate phase cone growth kinetics along dislocation pipes inside polycrystal grains. AIP Advances. 2018;8: 095202. https://doi.org/10.1063/1.5041728
18. Yarmolenko MV. Analytically Solvable Differential Diffusion Equations Describing the Intermediate Phase Growth. Metallofiz. Noveishie Tekhnol.. 2018;40(9): 1201-1207. https://mfint.imp.kiev.ua/article/v40/i09/MFiNT.40.1201.pdf
19. Mehrer H. Diffusion in Solids. New York: Springer; 2007. 651 p. http://users.encs.concordia.ca/~tmg/images/7/79/Diffusion_in_solids_Helmut_Mehrer.pdf
20. Braunovic M. and Alexandrov N. Intermetallic compounds at aluminum-to-copper electrical interfaces: effect of temperature and electric current. IEEE Transactions on Components, Packaging, and Manufacturing Technology: Part A. 1994;17(1): 78-85. doi: 10.1109/95.296372
21. Darken LS. Diffusion, mobility and their interrelation through free energy in binary metallic systems. Transactions AIME .1948;175: 184-201. http://garfield.library.upenn.edu/classics1979/A1979HJ27500001.pdf